The charge density distribution and antiferromagnetic properties of azurite Cu3[CO3]2(OH)2

Article *in* Physics and Chemistry of Minerals · August 2001

DOI: 10.1007/s002690100176 · Source: OAI

3 authors, including:

Elena L. Belokoneva
Lomonosov Moscow State University
249 PUBLICATIONS **2,077** CITATIONS

SEE PROFILE

Phys Chem Minerals (2001) 28: 498–507

ORIGINAL PAPER

E. L. Belokoneva · Yu. K. Gubina · J. B. Forsyth

The charge density distribution and antiferromagnetic properties of azurite $Cu_3[CO_3]_2(OH)_2$

Received: 8 September 2000 / Accepted: 6 March 2001

Abstract The structure and bonding in azurite are investigated on the basis of accurate single-crystal X-ray diffraction data. Both spherical IAM and pseudoatom models have been used in the refinements. The deformation electron density: dynamic (IAM) and static (pseudoatom) are mapped for the CO_3 group and for Cu(1) and Cu(2) squares in different sections. The carbonate group in azurite, not constrained to have trigonal symmetry, exhibits peaks in both static and dynamic maps which result from σ-bonds between C–sp^2 hybrid orbitals and O–p orbitals with some delocalisation of density in the dynamic map because of the thermal motion of oxygens. For the analysis of crystal fields and for the multipole calculations, coordinate systems on the Cu-atoms have been chosen as for a Jahn-Teller octahedron, but with the normal to the square as the *z*-axis instead of the absent apical oxygens. In both Cu squares there are peaks which result from single Cu–O σ-bonds. Most remarkable is the preferential occupation of the non-bonding 3d orbitals of Cu-atoms being above and below the Cu-squares. The centre of these peaks for the Cu(1)-atom makes an angle with the *c*-axis ~53° in the *ac* plane. This direction corresponds to the maximum magnetic susceptibility at ambient temperature. The real atomic charges of Cu-atoms in azurite determined from multipoles are close to Cu^{+1}. The occupancies of the 3d atomic orbitals show that non-bonding orbitals in both Cu-atoms are most populated, in contrast to bonding orbitals, as is typical for the Jahn-Teller octahedron. The absence of apical oxygens makes this effect even more pronounced. It is suggested that the antiferromagnetic structure below 1.4 K will be collinear and commensurate with $b' = 2b$.

Key words Azurite · Experimental charge density · Orbital occupation · Antiferromagnetic properties

E. L. Belokoneva (✉) · Yu. K. Gubina
Moscow State University,
Geological Faculty, Department Crystallography,
Vorobjevi Gory Moscow, 119899 Russia
Tel.: +7 (095) 939-4926; Fax: +7 (095) 932-8889
e-mail: elbel@geol.msu.ru

J. B. Forsyth
Clarendon Laboratory, Oxford University,
Parks Road, Oxford OXI 3PV UK

Introduction

The determination of the experimental electron density (ED) distribution from precise X-ray diffraction data offers the possibility to analyse the chemical bonding and its pecularities in crystals. Up till now, many compounds – both synthetic and natural – have been studied by this method, and in particular a large group of compounds containing tetrahedral anions such as silicates, phosphates and borates. In addition to tetrahedra, the borates may also contain triangular anionic groups. Amongst the carbonates, in which carbon is always trigonally coordinated and to which azurite belongs, only calcite, magnesite and dolomite have been investigated (Effenberger et al. 1983; Goettlicher and Vegas 1988; Maslen et al. 1995). The crystal structure of azurite was first determined by von Gattow and Zemann (1958) and refined using single-crystal neutron diffraction data by Zigan and Schuster (1972). Unlike in calcite, the carbonate group in azurite is not constrained to have trigonal symmetry. The Cu^{2+} ions are in square coordination with oxygen atoms from two carbonate and two hydroxyl groups. At low temperature, azurite exhibits antiferromagnetic properties (Frikkee and Van den Handel 1962).

We now report the refinement of the structure of azurite in which accurate single-crystal X-ray diffraction data have been used to obtain the charge density distribution by both IAM and multipole refinements that include the calculation of deformation electron density maps, the determination of atomic charges and the occupancies of the Cu^{2+} 3d orbitals. In the light of this analysis we have been able to add further detail to the

antiferromagnetic model of the azurite structure below its Néel temperature of 1.86 K, first proposed by Frikkee and Van den Handel (1962).

Experimental procedure

The sample for investigation was provided from the Ural deposit by the Vernadsky Geological museum of RAS, Moscow. A spherical specimen with radius 0.015 cm, prepared from dark blue crystal, was used for the data collection. The monoclinic unit-cell parameters were refined from 15 reflections measured using a Syntex P1 diffractometer (Table 1). The main dataset was collected in the hemisphere h^0_+, k^-_+, l^-_+, where 3008 reflections were measured in the region $2\theta = 5$–$100°$. Then a further 716 reflections were added in the region h^-_{-1}, k^-_+, l^-_+, $2\theta = 5$–$50°$. We used Mo–K_α radiation from a graphite monochromator and a variable scan angle increasing from 2° to 3° with increasing scattering angle. A variable scan rate from 2° to 12° min^{-1} depending on the intensity was used in the measurements. The stability was checked by periodic measurement of the (10–2) reflection intensity. The measurement lasted 150 h, during which the specimen was in the beam for 117 h. The drift in the primary beam intensity did not exceed 2.5%. Thus, we obtained eight equivalents in the region $2\theta = 5$–$50°$ and four in the region $2\theta = 5$–$100°$. The integrated intensities were determined by the Lehmann-Larsen procedure for peak profile analysis adopted in the program PROFIT (Streltsov and Zavodnik 1989). The averaging of all the data gave $R_{int.} = 0.0516$ for the $(F_{obs})^2$ of 1549 independent reflections with $F_{obs} \geq 4\sigma(F_{obs})$. The slightly high value of R_{int} reflects some asphericity in the shape of our sample. We applied corrections for LP and for absorbtion by the spherical sample ($\mu r = 1.62$).

Spherical refinement (IAM) and deformation density

As a starting point for the refinement using the CSD package (Akselrud et al. 1989), we took the atomic coordinates of von Gattow and Zemann (1958), which were then refined by least-squares with anisotropic thermal vibration parameters. The Cu form factor was corrected for the anomalous scattering of Mo radiation. An isotropic secondary extinction correction was applied following Zachariasen (1945), in which $R_x = 4300$ (the dimension of the mosaic block in Å).

Table 1 Crystallographic and experimental data

Space group	$12_1/c1$
a (Å)	5.011(2)
b (Å)	5.850(2)
c (Å)	10.353(4)
β (°)	92.41(3)
Cell volume, V (Å^3)	303.2(3)
Z	2
Calculated density, ρ_{calc} (g cm^{-3})	3.775(4)
Mean radius of single crystal, r (cm)	0.0150
Absorption coefficient, μ (5 cm^{-1})	108.27
Radiation and wavelength	Mo 0.71069
Diffractometer	Syntex P1
Scan type	$\omega - 2\theta$
$2\theta_{max}$ and $(\sin\theta/\lambda)_{max}$, (Å^{-1})	100.00 1.1
No. of measured reflections	3008
No. of unique reflections	1549

The deformation electron density was calculated from the difference Fourier series:

$$\delta\rho(\mathbf{r}) = (1/V)\sum[F_{obs}(q) - F_{IAM}(q)]\exp(-2\pi iq\mathbf{r}) \ .$$

To obtain the structural parameters corresponding to the independent atomic model (IAM) with spherically symmetrical scattering functions, the refinement was restricted to the 480 independent reflections having $\sin\theta/\lambda \geq 0.85$ Å^{-1}. With the weighting scheme $1/w = \sigma^2 + c(F_{obs})^2$, $c = 0.0002$, the refinement gave $R = 0.0176$, $R_w = 0.0231$, $S = 1.07$ (Table 2). Tables 3 and 4 give the final atom coordinates, anisotropic displacement parameters and selected interatomic distances and angles.

The crystal structure of azurite is well described by von Gattow and Zemann (1958). It is built from CO_3 triangles and Cu(1)–4O and Cu(2)–4O squares. The CO_3 group is not constrained by symmetry, in contrast to trigonal groups in calcite or dolomite. However, the triangle in azurite is sufficiently regular with the O–C–O angles close to 120° but the distance C–O(3) is enlarged (Table 4). The carbon atom lies practically in the same plane as the oxygens. The Cu(1) atoms lie at the centres of symmetry at the corners of the unit cell and at the middle of its *bc* face and are coordinated by O(1), O(2)-atoms at distances of ~1.94, 1.95 Å (Table 4). Next-nearest neighbours are a C-atom and other oxygens. The coordination of Cu(2) is also square (~1.93–1.99 Å, Table 4). There are two oxygens in the second coordination sphere at distances of 2.36 and 2.76 Å, but the coordination polyhedron is not described by von Gattow and Zemann (1958) as octahedral because these atoms do not lie on the normal to the square. A centre of symmetry lies at the middle point of common edge of two Cu(2) squares.

The connection of the square planar groups Cu(1) and Cu(2) in the chain along the *b* axis is shown in Fig. 1a. The normal to the Cu(1) plane lies close to the diagonal of the *ac* face or [101] (Fig. 1b). The orientation of the pairs of Cu(2) squares is also approximately diagonal [10–1] and perpendicular to the Cu(1) planes.

The deformation density $\delta\rho(\mathbf{r})$ was investigated in sections which include the CO_3 group and the Cu(1)–4O and Cu(2)–4O squares. Figure 2a shows the $\delta\rho(\mathbf{r})$ distribution in the plane defined by the centre of the oxygen atoms of the CO_3 triangle. Three peaks with maxima of 0.3–0.5 e/Å^3 result from σ-bonds between C–sp^2 hybrid orbitals and O–p orbitals. The heights of these peaks are close to the value 0.4 found in $CaCO_3$, but are not as symmetrical as in the trigonal carbonates mentioned above. Because of the delocalisation of the electron density, it is not meaningful here to comment on the presence or absence of the π-components in the C–O bonds.

Such a distribution of $\delta\rho(\mathbf{r})$ may result from the low symmetry of the CO_3 group in azurite, with the consequent inequivalence of O(2), O(3) and O(4) in bonding with other atoms in the structure, as well as from the thermal motion of the CO_3 group. The anharmonicity of

Table 2 Spherical and multipolar refinement results

Spherical (IAM) model refinement	
Restrictions	$F(\mathrm{hkl}) > 4.00\sigma(F)$
Weighting scheme, c	$1/[\sigma\,(\mathrm{F})^2 + 0.0002(F_{\mathrm{obs}})^2]$
Extinction formalism, R_x, Å	Zachariasen (secondary), 4300
$>\sin\theta/\lambda<$, (Å^{-1})	0.8–1.0
R_{hkl}	0.0176
R_{whkl}	0.0231
S	1.07
$>\sin\theta/\lambda<$, (Å^{-1})	0.0–1.0
R_{hkl}	0.0262
R_{whkl}	0.0328
S	2.48
Multipolar model refinement	
Weighting sheme, c	$1/[\sigma(\mathrm{F})^2 + (0.01F_{\mathrm{obs}})^2]$
Extinction formalism, g, Å $\times 10^4$, (seconds)	Becker-Coppens (Lorentz mosaic spread, type I) 0.0479(9), 6.85″
R_{hkl}	0.0169
R_{whkl}	0.0219
S	1.48
κ', P_{val} refinement	
R_{hkl}	0.0178
R_{whkl}	0.0230
S	1.44

	Cu	C	O	H
κ'	0.98(6)	1.04(1)	0.98(3)	1.14(8)

Atom	Cu(1)	Cu(2)	C	O(1)	O(2)	O(3)	O(4)	H
P_{val}	4.94(4)	10.17(2)	3.63(8)	6.47(3)	6.56(3)	6.52(3)	6.46(3)	0.74(8)

Table 3 Atomic fractional coordinates, anisotropic displacement amplitudes for Cu, C, O and isotropic displacement amplitudes for H after multipole refinements

Atom	x/a	y/b	z/c
Cu1	0	0	0
Cu2	−0.2503(3)	0.9985(3)	0.4166(1)
C	0.329(2)	0.300(2)	0.318(1)
O1	0.728(2)	0.811(2)	0.445(1)
O2	0.104(2)	0.399(2)	0.331(1)
O3	0.450(2)	0.208(2)	0.417(1)
O4	0.431(2)	0.296(2)	0.207(1)
H	0.180(2)	0.801(2)	0.369(1)

Atom	U^{11}	U^{22}	U^{33}	U^{12}	U^{13}	U^{23}
Cu1	0.01101(6)	0.00793(3)	0.00875(1)	−0.00154(8)	0.00066(4)	0.00088(4)
Cu2	0.00911(4)	0.00983(3)	0.00814(1)	0.00067(6)	−0.00128(2)	−0.00121(2)
C	0.0116(3)	0.0102(2)	0.0079(1)	0.0021(4)	−0.0002(2)	0.0006(2)
O1	0.0118(2)	0.0098(1)	0.01021(5)	0.0004(3)	0.0003(2)	−0.0012(1)
O2	0.0152(3)	0.0175(2)	0.01052(5)	0.0073(4)	0.0002(2)	−0.0009(2)
O3	0.0151(3)	0.0174(2)	0.00888(5)	0.0062(4)	0.0000(2)	0.0028(2)
O4	0.0144(2)	0.0173(2)	0.00857(5)	0.0043(4)	0.0019(2)	0.0030(2)
H	0.032(2)					

atomic displacements has been calculated using the Edgeworth model (International tables for X-ray crystallography 1969) adopted in CSD up to tensor of fourth rank. The coefficients obtained in the refinement were mostly less than twice their standard deviations. However, c233 = −0.018(9) for the carbon atom and several coefficients for oxygen atoms were: O(1) c113 = 0.06(2), d1111 = 0.05(2), d3333 = −0.0020(9), d1222 = −0.009(5); O(2) c111 = −0.39(9), c222 = −0.21(9), O(3) c111 = −0.26(9), c113 = −0.05(2), d1112 = 0.021(8), d1222 = 0.023(6), d1122 = 0.013(5), d1233 = 0.0022(7); O(4) c111 = 0.27(9), c222 = 0.17(9), c112 = 0.12(5), d1111 = 0.06(2), d2223 = −0.006(2). The same section of $\delta\rho(\mathbf{r})$ as in Fig. 2a demonstrates now a much more symmetrical distribution for the three peaks with the heights of 0.6 e/A^3 lying practically on C–O bond lines. Nevertheless, there are some abnormally high peaks in the region of the lone pairs of O(3) atom, thus the

harmonic approximation is more appropriate for our experimental data set. The $\delta\rho(\mathbf{r})$ distribution in the Cu squares is practically the same with and without anharmonicity.

Figure 3a shows a section through Cu(1) square defined by the centre of Cu(1), O(1), O(2) atoms. Four 0.3 $e/\text{Å}^3$ peaks in the corners are σ-bonds between Cu- and O-atoms. There is a large minimum of $\delta\rho(\mathbf{r})$ around Cu(1)-atom extended in the directions to the O(1), O(1′) ligands. Two small 0.2 $e/\text{Å}^3$ peaks are on diagonals between O(1) and O(2). Several other sections perpendicular to the Cu(1) square show that the main deformation density is concentrated above and below the Cu(1) square. The section of the Cu(1) square parallel to the *ac* face (Fig. 3b) contains the normal to the square plane. Two 1.1 $e/\text{Å}^3$ peaks at a distance of ~0.65 Å are due to the 3d electrons of the Cu(1) atom. Most remarkable for subsequent discussion is the angle (~53°) between the centre of these maxima and the *c*-axis (Figs. 3b, 1b).

Table 4 Selected interatomic distances and angles

Cu1	−O(2) 1.936(4)	−O(1) 1.947(3)	
	−O(2) 1.936(4)	−O(1′) 1.947(3)	
Cu2	−O(3) 1.935(3)	−O(1) 1.965(3)	
	−O(4) 1.940(4)	−O(1) 1.992(4)	
C	−O(2) 1.278(3)	−O(4) 1.279(4)	−O(3) 1.290(4)
∠O(2)–C-O(3)		119.6(3)^0	
∠O(2)–C-O(4)		119.5(3)^0	
∠O(3)–C-O(4)		120.9(3)^0	

In contrast to the distribution of $\delta\rho(\mathbf{r})$ in the Cu(1) square, the section through the Cu(2) square shows two 1.1 $e/\text{Å}^3$ peak maxima at a distance of ~0.65 Å in the square plane [diagonal direction between O(1) and O(1′), Figs. 4a, 1a]. The peaks with heights 0.7 and 0.5 $e/\text{Å}^3$ are on diagonals between O(1) and O(1′) and normal to the Cu(2) plane (Fig. 4b, c) in contrast to their absence on section Cu(2) and O(3) from the second coordination sphere. The 0.2–0.6 $e/\text{Å}^3$ peaks in the corners are due to σ-bonds between Cu and O atoms.

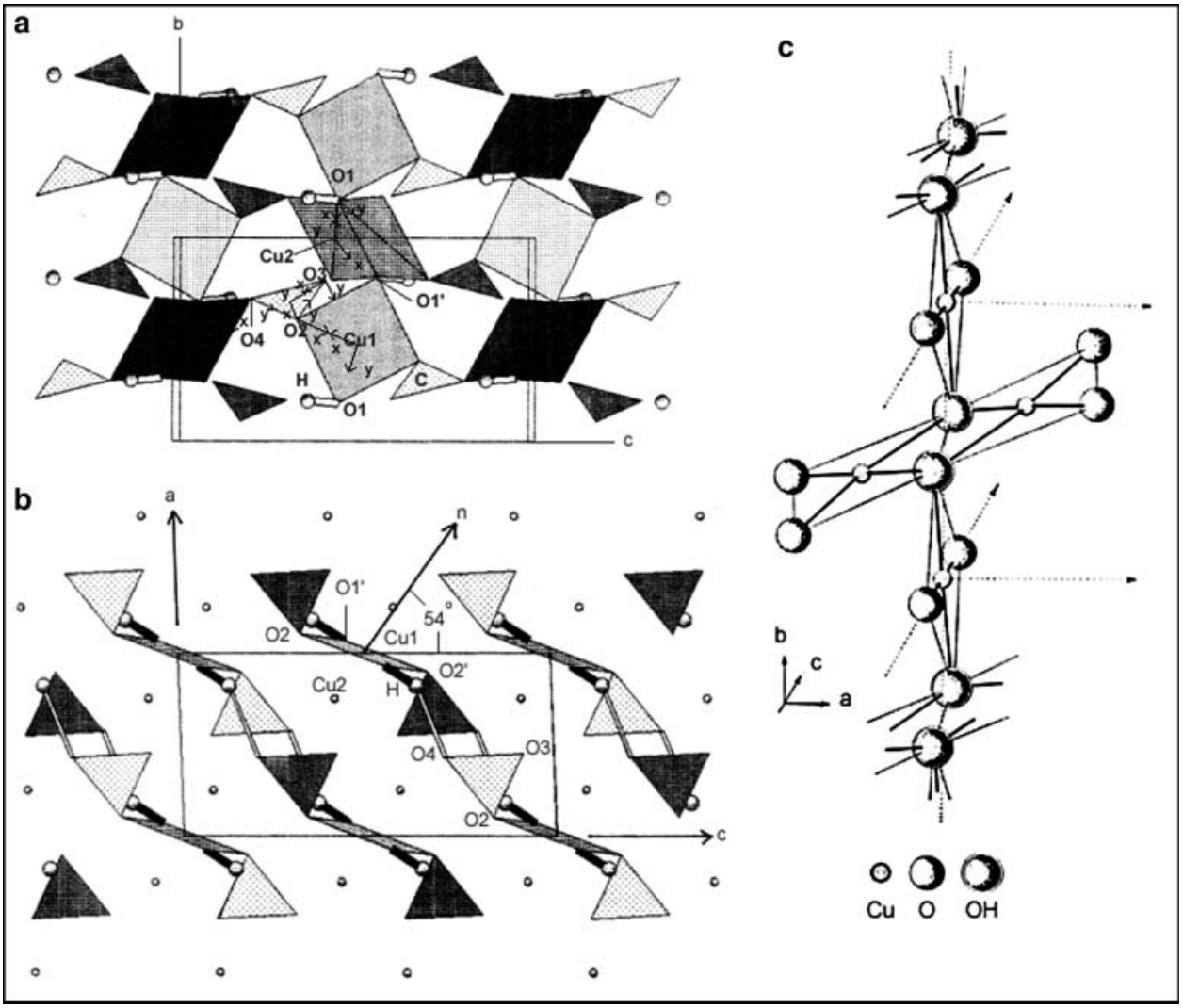

Fig. 1a, b Cu(1) and Cu(2) squares and C triangles arrangement in azurite crystal structure, the hydrogen atoms are shown as *spheres*. **a** *bc* projection, the *arrows* indicate coordination systems. **b** *ac* projection. **c** Cu chain from Gattow and Zemann (1958)

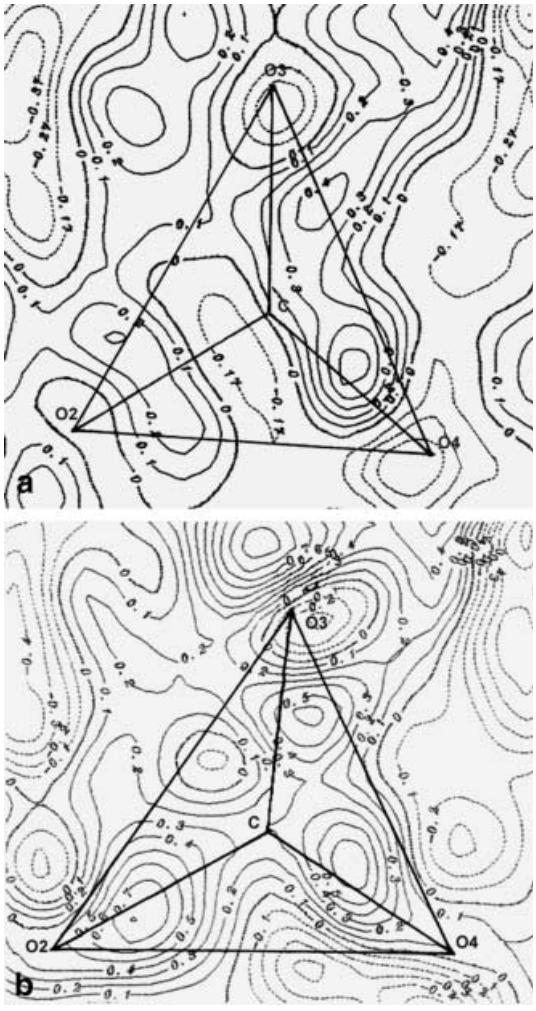

Fig. 2a, b Deformation density in CO_3 triangle. **a** The harmonic approximation of thermal vibration parameters. **b** The anharmonic approximation of thermal vibration parameters. Contour interval here and in the following maps for spherical refinement is 0.1 $e/\text{Å}^3$

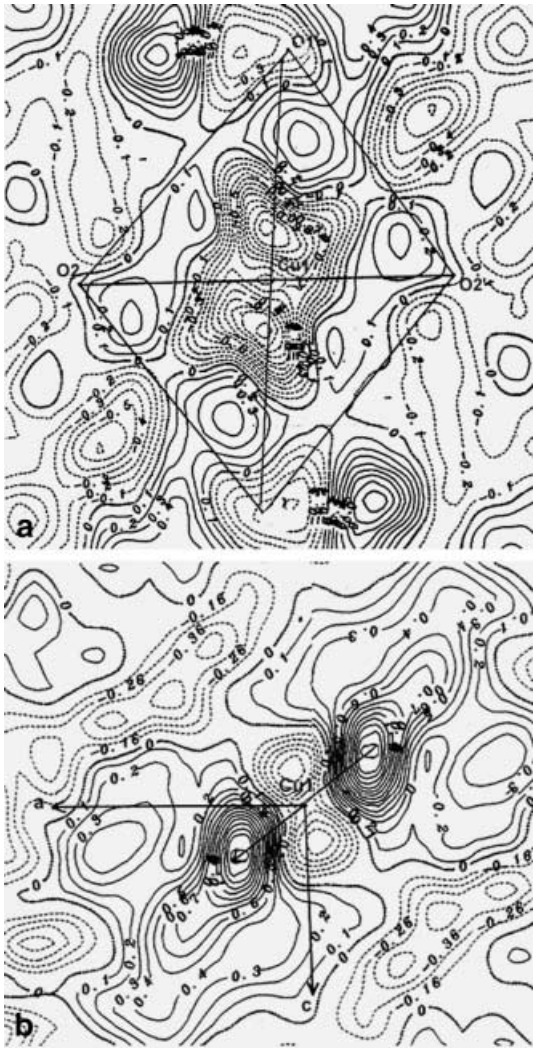

Fig. 3a, b Deformation density in Cu(1) square. **a** Section in the square plane. **b** Section parallel *ac* axis, close to perpendicular to the square

In the azurite structure the copper atoms are in principle divalent ($3d^9$ configuration). The typical Cu^{2+} ion coordination is a Jahn-Teller-distorted octahedron in which all 3d orbitals have a population of two save for $3d_{x^2-y^2}$ with one electron. In azurite there are only oxygen squares around Cu atoms and no apical ligands; nevertheless, we may approximate the crystal field at both Cu atoms as one formed by the four oxygens and the normal to this plane. The x, y coordination axes for Cu atoms are directed to the corners of the square and the z axis to its normal.

It is known that in a tetragonal point group D_{4h} the 3d energy levels are split into four levels corresponding to the orbitals: (d_{xz}, d_{yz}), (d_{xy}), ($d_{x^2-y^2}$), (d_{z^2}); for orthorhombic D_{2h} into six (d_{xz}), (d_{yz}), (d_{xy}), ($d_{x^2-y^2}$), (d_{z^2}), ($d_{z^2}/d_{x^2-y^2}$) and for monoclinic C_s into five (d_{z^2}), ($d_{x^2-y^2}$), (d_{xy}), (d_{xz}), (d_{yz}).

For the Cu(1) one may conclude on the basis of the $\delta\rho(\mathbf{r})$ distribution that in all approximations the d_{z^2}, d_{xz} and d_{yz} orbitals are most populated and these levels are stabilised, whereas the $d_{x^2-y^2}$ orbital is least populated relative to the spherical atom, and this level is destabilised as is typical for the Jahn-Teller octahedron. The absence of apical oxygens does not remove this effect, but makes it even more pronounced.

For the Cu(2) the positive lobe of the d_{xy} orbital is most populated (at the same time the negative lobe is depopulated), the d_{xz}, d_{yz} orbitals being slightly populated. As for Cu(1), the $d_{x^2-y^2}$ orbital is least populated and this level is destabilised. The most populated d_{xy} lobe is directed to the mid-point (symmetry centre) of the common edge O(1)–O(1′) between two Cu(2) squares.

The position of the hydrogen atom in azurite has been determined previously by Zigan and Schuster (1972) from neutron single-crystal data. Nevertheless, a large 0.8 $e/\text{Å}^3$ peak in $\delta\rho(\mathbf{r})$ outside the Cu(1) square (Fig. 3a) with coordinates $x = 0.846$, $y = 0.230$, $z = 0.623$ is clearly due to the single H electron. A comparison between the neutron and X-ray H

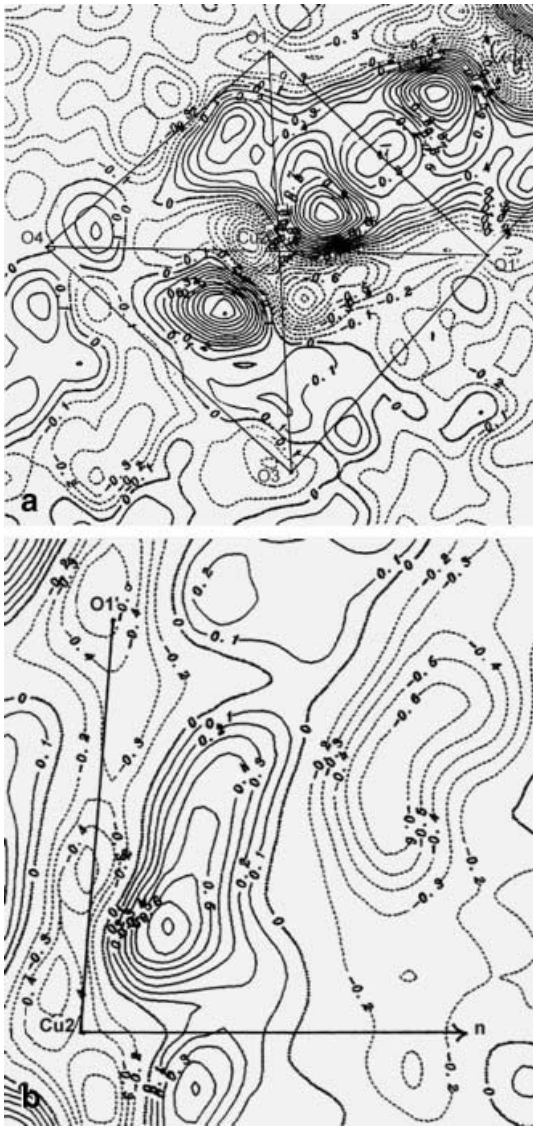

Fig. 4a, b Deformation density in Cu(2) square. **a** Section of the pair of Cu(2) and Cu(2′) squares and common edge O(1)–O(1′). **b** Section through the O(1′) and normal to the Cu(2) plane

coordinates shows that the latter imply a somewhat closer position of H to O(1) H–O(1) = 0.869 Å, H.....O(4) = 2.290 Å, than the neutron parameters: H–O(1) = 0.97 Å, H.....O(4) = 2.13 Å. The distance D–A: O(1)–O(4) = 3.00 Å corresponds to a weak hydrogen bond.

The section of $\delta\rho(\mathbf{r})$ in Fig. 5 defined by the centre of donor atom O(1), the H position from neutron parameters and the acceptor O(4) shows a typical hydrogen bond with the deformation density peak of 1.0 $e/\text{Å}^3$. The weak peak of 0.2 $e/\text{Å}^3$ is also in this map close to the O(4) acceptor. This bond connects O(1), common ligand for two Cu(2) and one Cu(1), with the O(4) belonging to the CO_3 triangle and another Cu(2) square, translated along the *a* axis (Fig. 1a, b). Thus, the weak hydrogen bond connects Cu(2) squares along *a*.

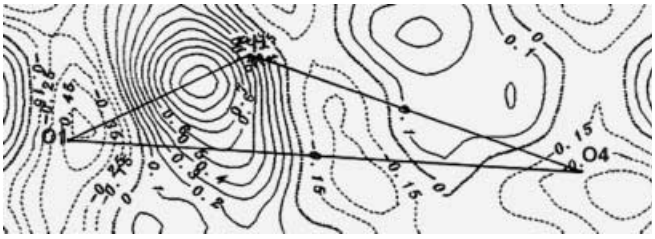

Fig. 5 Deformation density of the hydrogen bond O(1)–H.....O(4)

Pseudoatom refinement and static deformation density

A multipole refinement was undertaken to obtain electron-density characteristics undisturbed by the atomic thermal motion present in the static deformation density maps and to obtain the 3d-orbital populations of the Cu atoms. The same experimental data set corrected for absorbtion by a spherical sample was used as in the previous refinements. Structural parameters from the spherical model were used as starting values in the multipole refinement which was carried out with the program MOLDOS96 (J. Protas, personal communication) modified for DOS personal computers and based on the earlier program MOLLY (Hansen and Coppens 1978). The anharmonicity of the atomic displacements were modeled using a Gram-Charlier expansion up to tensor of fourth rank (International tables for X-ray crystallography 1974). All the coefficients obtained in the refinement were comparable with their standard deviations; thus we may conclude that there are no significant anharmonic motions in azurite.

In the Hansen and Coppens (1978) multipole model, the electron density is approximated as the sum of the pseudo-atomic electron densities in the form:

$$\rho_{\text{atomic}}(\mathbf{r}) = P_c\rho_{\text{core}}(\mathbf{r}) + P_v\kappa'^3\rho_{\text{valence}}(\kappa' r) + \sum_{l=1}^{4}\kappa''^3 R_l(\kappa'' r)\sum_{m=-1}^{1} P_{lm}y_{lm}(\mathbf{r}/r)$$

The refinable parameters were the scale factor, the valence-shell contraction–expansion parameters κ', κ'' and the multipole populations P_v and P_{lm} up to the hexadecapole level ($l_{max} = 4$). Isotropic secondary extinction was refined using Becker and Coppens' (1974) model with the assumption of mosaic spread domination (extinction type I) and with Lorentzian distribution of the mosaic block orientation. The form factors for the core and valence shells of neutral Cu, C, O and H were calculated from Hartree-Fock wave functions (Clementi and Roetti 1974). The anomalous dispersion coefficients were taken from the International tables for X-ray crystallography (1969). The multipole refinements were performed up to hexadecapoles for Cu, C, O and up to quadrupole for H. The exponential radial functions $r^{nl}\exp(-\kappa''\xi r)$ with $n_l = 4,4,6,8$ for Cu and with $n_l = 2,2,3,4$ for C, O, H were used. Initial values for the

orbital exponent coefficients $\xi_{Cu} = 8.2$, $\xi_C = 2.5$, $\xi_O = 4.5$, $\xi_H = 2.2$ were chosen following Hansen and Coppens (1978) and recent multipole refinements of related inorganic compounds (Ivanov et al. 1998, 1999, Kuntzinger and Ghermani 1999). One set of κ', κ'' parameters was used for both Cu(1) and Cu(2) and another for all the O atoms. At first, the scale factor, the positional and harmonic atomic displacement parameters and the extinction parameter were refined using all reflections. The weighting scheme $w = 1/[\sigma^2(F) + (cF)^2]$ with $c = 0.01$ provided the correct model fit according to the Abrahams and Keve (1971) criterion.

The asymmetric unit was constrained to be neutral during the refinement of P_v. The starting P_v parameters corresponded to the number of electrons in the valence orbitals of the atoms: 11.0 for Cu atoms [5.5 for Cu(1) taking into account the site symmetry multiplicity], 4.0 for the C atom, 6.0 for oxygen atoms and 1.0 for the H atom. The local coordinate systems on the Cu(1) and Cu(2) were chosen as described above: x and y to the corners of the square; on the C atom x and y were directed to O(2) and O(3) corners of triangle; on the oxygens x and y were directed wherever possible to the chemical bonds with cations or to other oxygens; on the hydrogen x was directed to O(1) (the donor atom in the hydrogen bond) and y parallel to the a axis (Fig. 1). Thus, the x and y axes were maximally orthogonal. The multipole refinement initially included the scale factor, positional and temperature anisotropic parameters, then κ' and P_v. In subsequent steps, the P_{lm}, and then the κ'' parameters were added to the refinement.

The agreement of the model obtained here was $R(F) = 0.019$, $S = 1.54$. The κ' parameters were equal to 1.00(1) for Cu atoms, 1.04(2) for C atom, 0.97(3) for O atoms, 1.21(1) for H. The P_v were equal to 5.17(4) for Cu(1), 10.67(1) for Cu(2), 3.56(1) for C, 6.34(4) for O(1), 6.42(4) for O(2), 6.36(3) for O(3), 6.30(3) for O(4), 0.67(9) for H, the charges corresponded to $Cu(1)^{+0.44}$, $Cu(2)^{+0.43}$, $C^{+0.44}$, $O(1)^{-0.34}$, $O(2)^{-0.42}$, $O(3)^{-0.36}$, $O(4)^{-0.30}$, $H^{+0.33}$ and were abnormally small.

In the case of pyrite, FeS_2 (Stevens et al. 1980), even negative charge on the Fe atom was obtained in refinements which included the Fe 4s electrons. As was mentioned there, the 4s population cannot be determined reliably from X-ray data because the diffuse 4s orbitals contribute significantly to only a few low-angle reflections that are also highly affected by extinction. Thus, the population of the Fe 4s density function has been fixed at zero. The multipole refinements of several Co-, Ni- and Mn-containing compounds carried out by Hollady et al. (1983) demonstrated that the models without 4s-density functions for Co, Ni, Mn atoms agreed better with theoretical expectations. The multipole refinement of $LiFePO_4$ (Streltsov et al. 1993) was also carried out with the assumption that the Fe 4s electrons are added to the oxygen valence shells. The novel investigation of CoS_2, NiS_2 and FeS_2 (Nowak et al. 1991) considered the model with Fe, Co and Ni as doubly charged cations, and P_v was thus 6, 7 and 8, respectively.

In the multipole refinement of natrolite (Ghermani et al. 1996) the charge of the sodium cation (+1) was never refined because of the sharpness of its 4s scattering function, which affects only very few low-order data. The same restriction was made for Li in α-spodumene (Kuntzinger and Ghermani 1999) and Ca in skolecite (Kuntzinger et al. 1998). Thus, this procedure is common in multipole refinements of alkali and alkali-earth compounds and it was adopted to overcome the same experimental problems in X-ray diffraction as were mentioned first for Fe in pyrites.

The high extinction in azurite (see Table 2), the very low charges in the first refinement and the method of attack discussed above lead us to make analogous assumptions. The starting P_v parameters for the four oxygen atoms in the structure were changed to 6.375 from 6.0 in order to take into account 1.5 4s electrons of both Cu atoms, whose starting P_v were 5 for Cu(1) and 10 for Cu(2), assuming that Cu 4s density functions are not included in the model.

The Cu(1) and Cu(2) positions in the azurite have Wyckoff notation 2a and 4e, respectively, and point symmetry $\bar{1}$ and 1. Nevertheless, an attempt was made to refine multipole population parameters under the constraints of higher symmetries: 4/*mmm*, *mmm* or *m*, being in the Cu planes. Thus, four different types of deformations were used for both Cu atoms: tetragonal, orthorhombic, monoclinic and, as it is in the structure, triclinic. The index-picking rules for site-symmetry spherical harmonics were taken from Kurki-Suonio (1977). The figures of merit R and S for four variants were: 0.0209, 1.76 (tetragonal), 0.0208, 1.71 (orthorhombic), 0.0205, 1.69 (monoclinic) and 0.0169, 1.44 (triclinic). There is no doubt that the approximation of higher symmetry is not correct in the case of azurite. At the end of the refinement seven weak reflections were rejected because $|Fo–Fc|/\sigma Fo > 15$. The extinction, positional and harmonic atomic displacement parameters were then refined again together with the multipole parameters without κ', κ''. The resulting atomic coordinates and anisotropic displacement parameters were found to be practically the same as those obtained from the spherical refinement (Table 3). Selected interatomic distances correspond to that given in Table 4.

The procedure of κ' refinement (only κ' and Pv) for net atomic charge determination was also performed (the κ' and P_v parameters are given in Table 2). It was found that κ' values are mostly close to 1: Cu atoms have κ' parameter equal to 1, thus are neither expanded, nor contracted; the carbon atom is somewhat contracted, and the hydrogen atom shows the maximum contraction; the oxygen atoms are expanded (Table 1). The charges correspond: Cu(1) + 1.11(4), Cu(2) + 0.83(6), C + 0.37(8), H + 0.26(8), O(1) − 0.47(4), O(2) − 0.57(4), O(3) − 0.53(3), O(4) − 0.46(3). One may conclude that 4s electrons of Cu atoms are involved in σ-bonding, thus the valence state of copper atoms is close to Cu^{1+}.

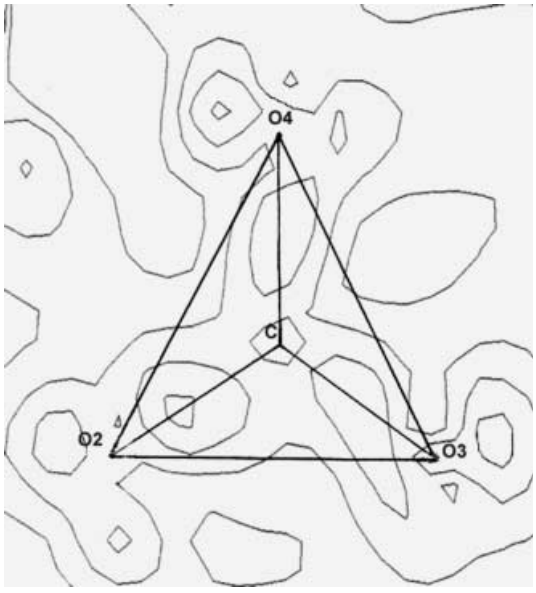

Fig. 6 Static deformation density in CO_3 triangle. Here and in the following maps contour interval is 0.2 $e/Å^3$

The static deformation electron density calculations were carried out using the program SALLY (Hansen, personal communication). The section of the CO_3 triangle (Fig. 6 is analogous to Fig. 2a, b) looks more "ideal" and symmetrical than that of the dynamic spherical model. There are three 0.4–0.6 $e/Å^3$ peaks being practically on C–O bond lines and oxygen lone pairs of the same highs. Nevertheless, it is not fully $3m$ symmetry as for CO_3 group in $CaCO_3$ and $MgCO_3$ obtained in VALRAY multipole refinement (V. A. Streltsov, personal communication 2000) for synchrotron data (Maslen et al. 1995) with the peak on C–O bond of 0.5 $e/Å^3$.

The sections of Cu(1) square confirms the principal characteristics of density distribution with its maximal concentration above and below the Cu(1) square on section Fig. 7a analogue to Fig. 3b, whereas the section of the Cu(1) square in the plane has only two weak peaks (Fig. 7b, analogue to Fig. 3a). There are large peaks in the plane of a couple of Cu(2)–Cu(2′) squares (Fig. 8a analogue to Fig. 4a). The hydrogen bond is shown in Fig. 9 analogue to Fig. 5.

The calculation of orbital populations was carried out for Cu(1) and Cu(2) on the base of the relations between multipole population parameters and 3d orbital occupancies for transition metal atoms derived by Holladay et al. (1983). The electron population of five 3d orbitals of the Cu(1) and Cu(2) atoms in the lowest symmetry variant are compared with spherically averaged free atom (Table 5). For the Cu(1) d_{xz} and d_{yz} orbitals are most populated: 31 and 28% in comparison with 20% for the spherical atom. Because of the absence of apical oxygen, they correspond to non-bonding orbitals. The bonding $d_{x^2-y^2}$ orbital is least populated (~8%), as was found in deformation density maps on the basis of a spherical

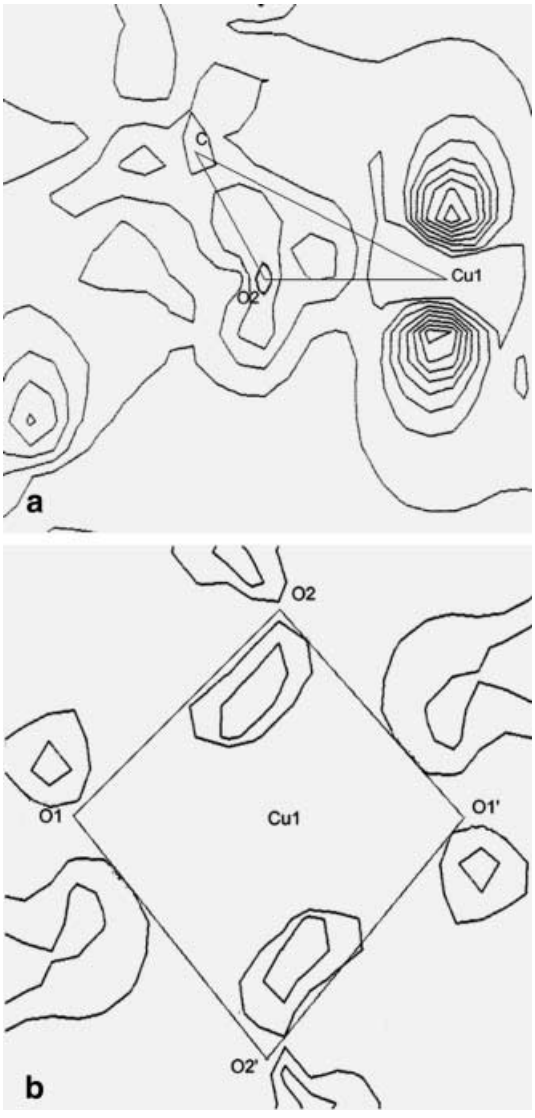

Fig. 7a, b Static deformation density in Cu(1) square. **a** Section via Cu(1), O(1) and C atoms close to perpendicular to Cu(1) square. **b** Section in the Cu(1) plane

model. For the Cu(2) atom also non-bonding d_{xz} and d_{xy} orbitals are mostly populated (25 and 26%), whereas the bonding $d_{x^2-y^2}$ and two non-bonding d_{z^2} and d_{yz} orbitals are depopulated. The difference in the populations of d_{yz} and d_{xz} orbitals may be due to electrostatic interactions between the negative ligands and the negative d-electron on orbitals. The interatomic distance Cu(2)–O(1′) is 1.992 Å in contrast to Cu(2)–O(1), which is less, 1.965 Å. In accordance with the choice of local coordination system, the interelectron repulsion is considerably less for electrons in the d_{xz} orbital [diagonal between O(1′) and normal to the Cu(2) square] and O(1′), than for electrons in the d_{yz} orbital [diagonal between O(1) and normal to the Cu(2) square] and O(1).

Thus, the investigation of the electron-density distribution in the azurite using both spherical (IAM) and pseudoatom (multipole) models leads to the following conclusions about chemical bond peculiarities:

As in other carbonates, in the carbon triangle there are single C–Oσ-bonds between C sp^2 hybrid orbitals and O–p orbitals; low symmetry and thermal motion of oxygens lead to some delocalisation of density.

In the Cu squares there are single Cu–O bonds; most remarkable is the preferable occupation by 3d electrons, the non-bonding orbitals of Cu atoms being above and below Cu(1), Cu(2) squares and in the direction of the common edge of Cu(2) pairs of squares.

The bridge of density in Fig. 8a through the common edge of two Cu(2) squares is well comparable with the bridge of density through the common edge of two Fe octahedra in the magnetite Fe_3O_4 structure. The last result was obtained in SCF–X_α calculations for the $(Fe_2O_{10})^{15-}$ cluster by Sherman (1987) and was explained in the assumption of antiferromagnetic coupling of iron cations.

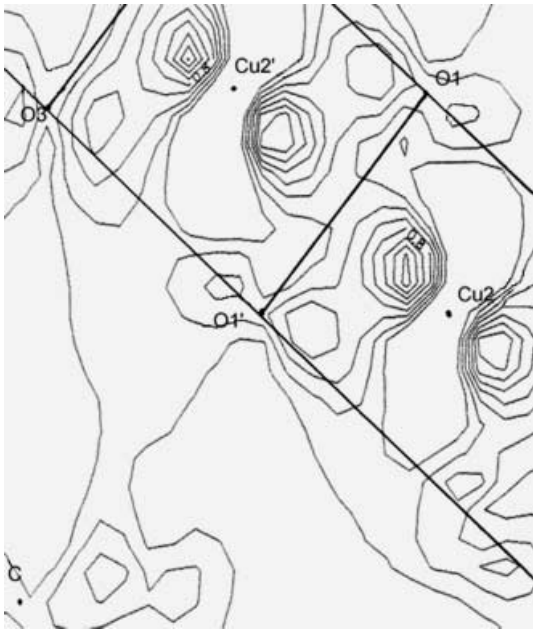

Fig. 8 Static deformation density in Cu(2)–Cu(2′) pairs with the common edge O(1)–O(1′) and O(3) atoms

Antiferromagnetic properties and the charge density of azurite

The magnetic behaviour of azurite received considerable attention some 40 years ago. The transition from paramagnetic to antiferromagnetic state at $T_N = 1.86$ K was first observed by Spence and Ewing (1958) by means of nuclear magnetic resonance and subsequently confirmed by a number of authors (Van der Lugt and Poulis 1959; Garber and Wagner 1960). A λ-type anomaly in the specific heat at $T = 1.84$ K was reported by Forstat et al. (1959). The associated entropy change of 1.17 cal $deg^{-1}mol^{-1}$ corresponds approximately to Rln2, implying that only one third of the copper moments order at this temperature.

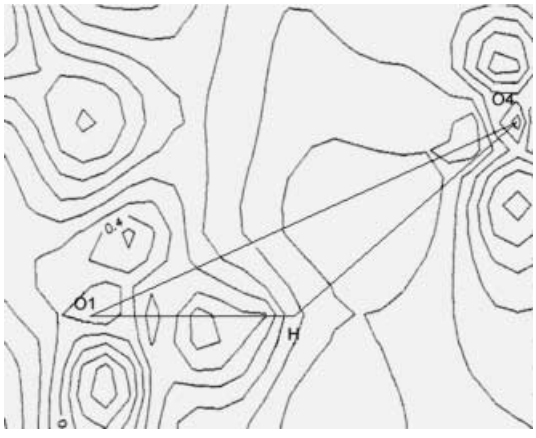

Fig. 9 Static deformation density on the hydrogen bond O(1)–H.....O(4)

Table 5 Orbital populations for Cu(1) and Cu(2) atoms in azurite

Orbital	Cu(1)		Cu(2)		Spherical atom Cu	
	Multipole refinement	Occupancies (%)	Multipole refinement	Occupancies (%)	Multipole refinement	Occupancies (%)
d_{z^2}	1.3(1)	13.1	1.9(1)	18.6	2	20
d_{xz}	3.1(2)	31.3	2.5(2)	24.6	2	20
d_{yz}	2.8(2)	28.3	1.3(2)	12.7	2	20
$d_{x^2-y^2}$	0.8(2)	8.1	1.9(2)	18.6	2	20
d_{xy}	1.9(2)	19.2	2.6(2)	25.5	2	20
Σd	9.9		10.2		10	20
$d_{z^2/xz}$	−0.7(1)		−0.4(2)			
$d_{z^2/yz}$	−0.1(2)		1.3(2)			
d_{z^2/x^2-y^2}	0.3(2)		1.0(2)			
$d_{z^2/xy}$	0.5(2)		−2.8(2)			
$d_{xz/yz}$	−1.3(2)		0.0(2)			
d_{yz/x^2-y^2}	−0.2(2)		0.8(2)			
$d_{zz/yz}$	1.9(3)		0.0(3)			
d_{zz/x^2-y^2}	−0.9(3)		−0.7(3)			
$d_{yz/xy}$	−1.5(2)		−0.3(2)			
$d_{x^2-y^2/xy}$	−1.4(2)		1.1(2)			

Frikkee and Van den Handel (1962) determined that the maximum of magnetic susceptibility lies in the a–c plane, c' making an angle of 52° to c in β-obtuse at 4.2 K. The angle to c increases as a function of decreasing temperature from 47° at temperatures above 14 K to some 50° at 1.4 K. The susceptibility χ obeys a Curie-Weiss law in the temperature interval 67–300 K, but then exhibits a broad maximum around 5 K. Below T_N, $\chi_{c'}$ tends to a small value, as would be expected for antiferromagnetic spin alignment in the c' direction. Frikkee and Van den Handel (1962) concluded that the most likely magnetic coupling scheme in azurite is one in which pairs of Cu(2) ions are coupled antiferromagnetically well above T_N but no long-range order is established. Below T_N the moments at the Cu(1) atoms form an ordered antiferromagnetic array. If we relate these ideas to the disposition of the Cu(1) and Cu(2) ions in the crystal structure and the results of the ED investigation, we see that the pairs of Cu(2) atoms related by centres of symmetry are likely to form antiferromagnetic dimmers through indirect exchange via O(1) and O(1)′. Although the shortest Cu(1)–Cu(1′) distance is a (5.011 Å), no simple superexchange path exists in this direction. We may therefore suppose that the most likely antiferromagnetic coupling Cu(1)–Cu(1′) may be established between Cu(1) ions separated by b (5.85 Å) via exchange paths involving the Cu(2) dimmers. We therefore suggest that the antiferromagnetic structure will be commensurate with $b' = 2b$ and with the Cu(1) moments of spin-ordered electrons (maximal deformation density peak) making an angle in the a–c plane of some 52° to c in β-obtuse. Weak magnetic coupling between the Cu(1), Cu(2) chains (Fig. 1) may occur through the carbonate complex anions.

Acknowledgements We thank the Vernadsky Geological Museum of RAS, Moscow, for providing the sample for the investigation, Professor Jean Protas for the use of MOLDOS96 and Professor Niels Hansen for the use of SALLY, Dr. Yury Abramov for the use of the program for the calculation of the 3d-orbital populations and Dr. Victor Streltsov for sending us a static density maps of CO_3 group in calcite for the comparison.

References

Abrahams SC, Keve ET (1971) Normal probability plot analysis of error in measured and derived quantities and standard deviations. Acta Crystallogr (A) 27: 157–165

Akselrud LG, Grin YuN, Zavalii PYu, Pecharsky VK, Fundamensky VS (1989) CSD universal program package for single-crystal and/or powder structure refinement IBM PC-DOS, ECM XII, Moscow, Coll. Abstr. 3, 155

Becker PJ, Coppens P (1974) Extinction within the limit of validity of the Darwin transfer equations. 1. General formalisms for primary and secondary extinction and their application to spherical crystals. Acta Crystallogr (A) 30: 129–147

Clementi E, Roetti C (1974) At. Data Nucl. Data Tables 14: 177–178. Academic press, New York

Effenberger H, Kirfel A, Will G (1983) Electronendichteverteilung im Dolomite $CaMg(CO_3)$ Tschermaks Min Petrol Mitt 31: 151–164

Frikkee E, Van den Handel J (1962) The magnetic behaviour of azurite. Physica 28: 269–276

Forstat H, Taylor G, King BR (1959) Low-temperature heat capacity of azurite. J Chem Phys 31: 929–931

Garber M, Wagner R (1960) Letter to the editor: the susceptibility of azurite. Physica 26: 777

Gattow G von, Zemann J (1958) Neubestimmung der Kristallstruktur von Azurite, $Cu_3(OH)_2(CO_3)_2$. Acta Crystallogr 11: 866–872

Ghermani NE, Lecomte C, Dusausoy Y (1996) Electrostatic properties in zeolite-type materials from high-resolution X-ray diffraction: the case of natrolite. Phys Rev (B),vol. 53, 9: 5231–5239

Goettlicher S, Vegas A (1988) Electron density distribution in magnesite ($MgCO_3$). Acta Crystallogr (B) 44: 362–367

Hansen NK, Coppens P (1978) Testing aspherical atom refinements on small-molecule data sets. Acta Crystallogr (A) 34: 909–921

Holladay A, Leung P, Coppens P (1983) Generalized relations between d-orbital occupancies of transition-metal atoms and electron-density multipole population parameters from X-ray diffraction data. Acta Crystallogr (A) 39: 377–387

International Tables for X-ray Crystallography (1969) International Union of Crystallography, Kynoh press, Birmingham, England

Ivanov YuV, Belokoneva EL, Protas J, Hansen NK, Tsirelson VG (1998) Multipole analysis of the electron density in topaze using X-ray diffraction data. Acta Crystallogr (B) 54: 774–781

Ivanov YuV, Zhurova EA, Zhurov VV, Tanaka K, Tsirelson VG (1999) Electron density and electrostatic potential of $KNiF_3$: multipole, orbital and topological analyses of vacuum-camera-imaging plate and four-circle diffractometer data. Struct Sci 55: 923–930

Kuntzinger S, Ghermani NE (1999) Electron density distribution and Madelung potential in α-spodumene, $LiAl(SiO_3)_2$, from two-wavelength high-resolution X-ray diffraction data. Acta Crystallogr Struct Sci 55: 273–284

Kuntzinger S, Ghermani NE, Dusausoy Y, Lecomte C (1998) Distribution and topology of the electron density in the aluminosilicate compound from high-resolution X-ray diffraction data: the case of scolecite. Acta Crystallogr (B) 54: 867–881

Kurki-Suonio K (1977) IV. Symmetry and its implications. Isr J Chem 16: 115–123

Maslen EN, Streltsov VA, Streltsova NR (1995) Electron density and optical anisotropy in rhombohedral carbonates. III. Synchrotron X-ray studies of $CaCO_3$, $MgCO_3$ and $MnCO_3$. Acta Crystallogr (B) 51: 929–939

Nowack E, Schwarzenbach D, Hanh T (1991) Charge densities in CoS_2 (pyrite structure). Acta Crystallogr (B) 47: 650–659

Sherman DM (1987) Molecular orbital (SCF–X_α–SW) theory of metal-metal charge transfer processes in minerals.1. Application to $Fe^{2+} \rightarrow Fe^{3+}$ charge transfer and "electronic delocalisation" in mixed iron oxides and silicates. Phys Chem Miner 14: 355–363

Spence RD, Ewing RD (1958) Evidence for antiferromagnetism in $Cu_3(CO)_3(OH)_2$. Phys Rev 112: 1544–1545

Stevens D, De Lucia ML, Coppens P (1980) Experimental observation of the effect of crystal-field splitting on the electroan density of iron pyrite. Inorg Chem 19: 813–820

Streltsov VA, Zavodnik VE (1989) The procedure of reconstruction of the integral intensities using diffraction profiles. Sov Phys Crystallogr 34: 1369–1375

Streltsov VA, Belokoneva EL, Tsirelson VG, Hansen NK (1993) Multipole analysis of the electron density in triphylite, $LiFePO_4$, using X-ray diffraction date. Acta Crystallogr (B) 49: 147–153

Van der Lugt W, Poulis NJ (1959) Proton magnetic resonance in azurite. Physica 25: 1313–1320

Zachariasen WH (1945) Theory of X-ray diffraction in crystals. New York

Zigan F, Schuster HD (1972) Verfeinerung der Struktur von Azurite, $Cu_3(OH)_2(CO_3)_2$, durch Neutronenbeugung. Z Kristalogr Kristallgeom Kristallphys Kristallchem 135: 416–436